

Instabilities of complex fluids with partially structured and partially random interactions

Giorgio Carugno^{1,2}, Izaak Neri^{1,3}, Pierpaolo Vivo^{1,4}

¹ Department of Mathematics, King's College London, Strand, London, WC2R 2LS, UK

E-mail: ²giorgio.carugno@kcl.ac.uk, ³izaak.neri@kcl.ac.uk,
⁴pierpaolo.vivo@kcl.ac.uk

Abstract. We develop a theory of thermodynamic instabilities for complex fluids composed of many interacting species organised in families. This model includes partially structured and partially random interactions and can be solved exactly using tools from random matrix theory. Depending on the parameters of the model, we detect and characterise analytically family condensation, family demixing at finite critical density, and random demixing. We apply the theory to phase separation of proteins triggered by a change of pH.

Keywords: Phase separation, Random Matrix Theory, Block structure, Fluid Instabilities

1. Introduction

Eukaryotic cells are compartmentalised into membrane-bound regions called organelles. Recently it was found that the cytoplasm also contains membraneless organelles that form through liquid-liquid phase separation and are important for various physiological processes [1].

Liquid-liquid phase separation in the cytoplasm is reminiscent of phase separation of a mixture of oil and water [2], but there are also a couple of important distinctions. Notably, the cytoplasm is composed of a large number of distinct macromolecules [3], e.g., human cells contain about 10^9 proteins from about 10^4 protein coding genes [4]. Although phase separation of two component mixtures, such as oil and water, is well understood, little is known about the physical principles that govern phase separation of fluids composed of a large number of distinct molecular species [5–8]. The latter problem is also of interest in other contexts, such as, for the formation of lipid rafts and clusters of receptors on the cell membrane [9–11], the assembly of protein complexes [12], the study of polydisperse fluids [13–15], the dynamics of interfaces in crude oil/brine mixtures [16], and the nucleation of iron in the mantle [17].

In an attempt to describe phase separation in a complex fluid, Sear and Cuesta [5] considered a fluid of N components described by a matrix of second order virial coefficients that is random. Building on random matrix theory [18,19], they found two possible instabilities of the homogeneous state leading to phase separation of the fluid: one akin to a liquid-vapour coexistence, where the composition of coexisting phases is similar but the total density differs (*condensation*); the other akin to the coexistence of water and oil, where the compositions of the two phases are very different (*demixing*).

Although very successful in predicting possible transitions within a fairly simple and elegant framework, the model in [5] presents some important drawbacks: (i) while condensation happens at a finite critical density, demixing happens at a total density diverging as \sqrt{N} . In other words, the Sear-Cuesta liquid composed of a large number of constituents – for any practical purpose – never demixes; (ii) The interaction between species is assumed to be *structureless*, which neglects important factors playing a role in the affinity/repulsion between molecules observed in reality. For example, (a) the number and geometry of interaction sites in proteins [20], and (b) features of the solvent, such as the pH and salt concentration, which affect the fluid particles' net charge.

In order to overcome the above drawbacks, we introduce in this work a model of a complex fluid containing a matrix of virial coefficients that is partially random and partially structured. This model allows us to embed physically motivated constraints in an otherwise random model, and to derive analytic conditions for the critical density and the nature of the instability. As we will show, in a partially random and partially structured model a complex fluid can demix at finite critical density, which is consistent with what is observed in experiments in cell biology.

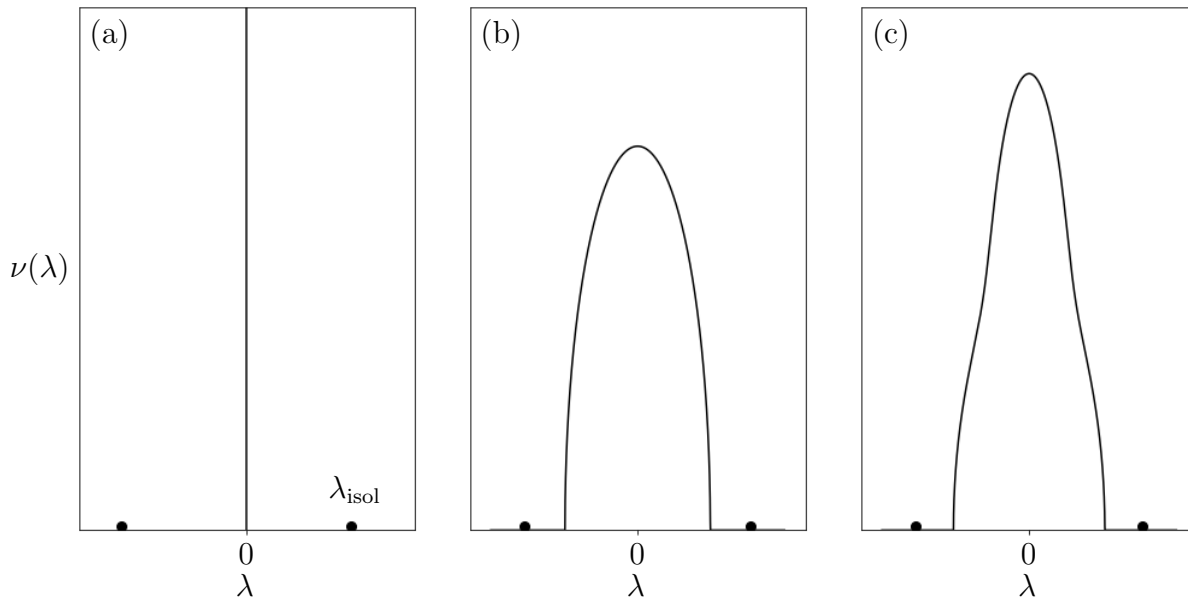


Figure 1. Comparison between the spectra of large matrices of the form (4) without disorder (a), with uniform disorder (b), and with non-uniform disorder (c) (see derivation in Appendix A). The solid black line denotes the distribution of eigenvalues and the black dots denote isolated eigenvalues. Parameters are set to $F = 2$, $\mu_{11} = 5$, $\mu_{12} = -10$, $\mu_{22} = -5$, and $c_1 = 0.4$. The noise amplitudes are (a) zero amplitude, (b) uniform noise with variance $\sigma^2 = 3N$, (c) non-uniform noises $\sigma_{11}^2 = 2N$, $\sigma_{12}^2 = N$, $\sigma_{22}^2 = 5N$. The scaling with N ensures that both the edges of $\nu(\lambda)$ and outliers are of the same order for large N .

2. Thermodynamics of complex fluids

We consider a fluid mixture at equilibrium composed of N chemical species with number densities ρ_i , $i = 1, 2, \dots, N$. The free energy density f of a homogeneous liquid in the dilute limit is well approximated by a second order virial expansion leading to the expression [21–25]

$$\beta f = \sum_{i=1}^N \rho_i (\log \rho_i - 1) + \frac{1}{2} \sum_{i,j=1}^N \rho_i B_{ij} \rho_j, \quad (1)$$

where β is the inverse temperature (which we set to $\beta = 1$ without loss of generality) and the matrix elements B_{ij} are the second order virial coefficients.

We aim to characterise the region of instability of the homogeneous phase towards a heterogeneous mixture. A phase of density $\vec{\rho} = (\rho_1, \dots, \rho_N)$ is unstable if the Hessian $H_{ij} = \partial_{\rho_i} \partial_{\rho_j} f$ of the free energy evaluated at $\vec{\rho}$ has at least one negative eigenvalue. The boundary of the unstable region in the space of parameters $\vec{\rho}$ is called the *spinodal* [26]. The spinodal is characterised by the smallest eigenvalue of H_{ij} being zero.

For the free energy in (1) the Hessian takes the simple form $H_{ij} = B_{ij} + \delta_{ij}(1/\rho_i)$. For simplicity, we consider the reference state $\vec{\rho}_0 = (\rho/N, \dots, \rho/N)$ for which all densities ρ_i are equal to ρ/N with ρ the total density. In this case, the density at the spinodal ρ_c , i.e. the total density above which the homogeneous state of the fluid is unstable, is

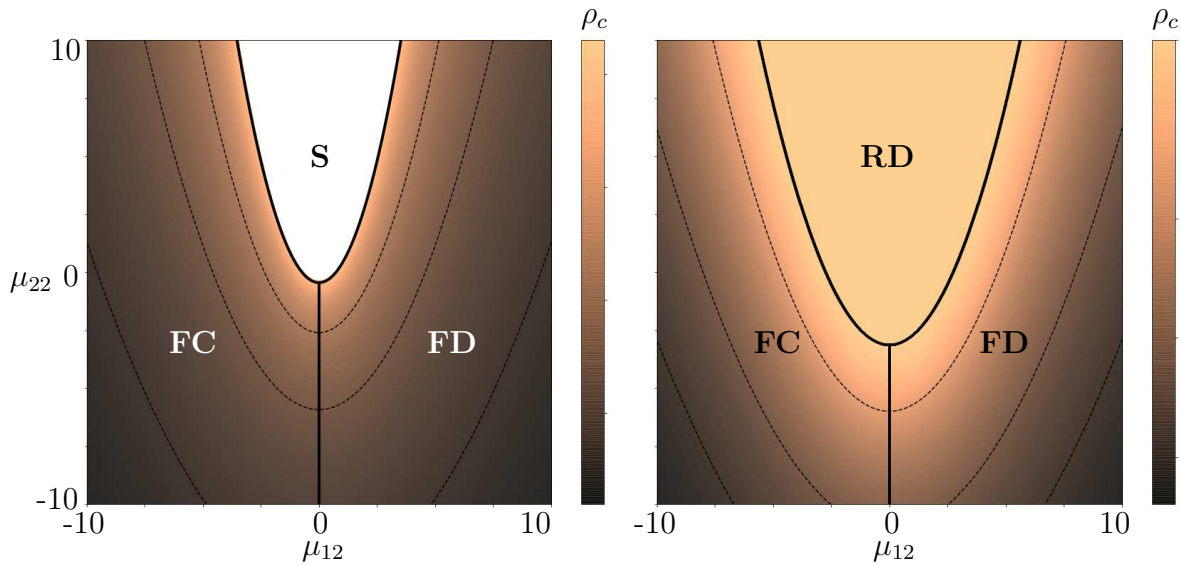


Figure 2. Comparison between the spinodals of complex fluids with deterministic interactions (left) and those with random interactions (right). The thick line separates different types of instability, in particular, family condensation (**FC**), family demixing (**FD**), random demixing (**RD**), and a region of stability (**S**) in white, and the thin lines denote contours of constant ρ_c . In the left picture, the color bar is in logarithmic scale. Parameters are $F = 2$, $\mu_{11} = 1$ and $c_1 = 0.7$, $\sigma_{11} = \sigma_{21} = \sigma_{22} = 0$ (left), $\sigma_{11}^2 = N$, $\sigma_{12}^2 = 0.5N$, and $\sigma_{22}^2 = 1.5N$ (right), where N is the number of species.

given by

$$\rho_c = -\frac{N}{\lambda_-}, \quad (2)$$

where $\lambda_- < 0$ is the smallest eigenvalue of \mathbf{B} .

To characterise the nature of a spinodal instability we use the local demixing angle θ defined as

$$\theta = \min\{\tilde{\theta}, \pi - \tilde{\theta}\}, \quad \tilde{\theta} = \arccos\left(\frac{\vec{1} \cdot \vec{v}^-}{\sqrt{N}|\vec{v}^-|}\right), \quad (3)$$

where \cdot is the dot product, $\vec{1}$ is the unit N -dimensional vector, and \vec{v}^- is the eigenvector of \mathbf{B} corresponding to the smallest eigenvalue λ_- .

There exist two extreme classes of fluid instabilities [5,7]: (i) *condensation* at $\theta = 0$ for which the two daughter phases have the same composition with a different total density, akin to a liquid-vapor phase transition; and (ii) *demixing* at $\theta = \pi/2$ for which two daughter phases have fully distinct compositions, akin to a mixture of water and oil. Intermediate situations are characterised by a value of $\theta \in (0, \pi/2)$.

The local demixing angle θ – strictly speaking only meaningful *at the onset* of a spinodal transition – is effective in predicting the type of instability at equilibrium [7], even though it can be quantitatively different from the “final” angle [15]. Given a sensible model for the interaction matrix \mathbf{B} , spinodal instabilities depend therefore only on its smallest eigenvalue and associated eigenvector.

3. Partially structured and random virial coefficients

In line with a long tradition of modelling complex systems with random matrices [5,18,27,28], we can replace the unknown virial coefficients between the chemical species with random interactions. From a modelling perspective it is however desirable to include generic properties of the interactions between the chemical species into the model. To this aim, we assume that the components of the fluid can be grouped into a small number of F families according to their characteristics, such as their charge or their hydrophobicity, and we assume that the statistical properties of the intra- and inter-family interactions are known. In other words, we assume that the properties of the virial matrix on the coarse-grained level of families are known, while the detailed microscopic interactions are unknown.

Mathematically, we describe a partially structured and random model with a virial matrix of the form

$$\mathbf{B} = \mathbf{D} + \mathbf{C} * \mathbf{Z} , \quad (4)$$

where \mathbf{D} and \mathbf{C} are deterministic rank- F matrices representing the coarse-grained knowledge we have about the interactions between families, and \mathbf{Z} is a random matrix that represents our ignorance about the microscopic interactions. The symbol $*$ is the element-wise product. We label the indices such that the matrices \mathbf{D} and \mathbf{C} have a block structure, in particular, $D_{ij} = \mu_{s(i)s(j)}$ and $C_{ij} = \sigma_{s(i)s(j)}$, where $s(i) \in \{1, 2, \dots, F\}$ is a function that keeps track of which family s a given index i belongs to. We use the convention that $s(i) = s$ for all $i \in \{\sum_{t=0}^{s-1} N_t + 1, \dots, \sum_{t=0}^s N_t\}$ where N_s denotes the number of species that belong to family s and $N_0 = 0$. The entries of \mathbf{Z} are independent and identically distributed random variables with mean 0 and variance 1. For $F = 1$ we recover the model of Sear and Cuesta [5]. Partially random and partially structured random matrices have been studied before in the context of neural networks [29,30], but those models are nonsymmetric.

4. Spectral properties of large random matrices

The spectrum of an infinitely large matrix of the form (4) consists of two parts, a continuous spectrum determined by the random matrix $\mathbf{C} * \mathbf{Z}$ and a finite number of at most F outlier eigenvalues λ_{isol} that are determined by the deterministic matrix \mathbf{D} (see figure 1): depending on the scaling with N of the moments of B_{ij} , outliers can be influenced by the noise. The smallest eigenvalue λ^- is either located at the lower edge of the continuous spectrum or is one of the outliers. The associated eigenvector \vec{v}^- , and thus the nature of the instability, has different properties in the two cases.

In the following we will discuss the fluid instabilities in three versions of the model (4) with increasing complexity in the matrix \mathbf{C} of noise amplitudes: (i) the deterministic case with zero noise amplitudes; (ii) the case with uniform noise amplitudes, $\mathbf{C} = \sigma \mathbb{1}$, where $\mathbb{1}$ is the identity matrix; (iii) the general case. Subsequently, we illustrate the

general formalism in the case of two families $F = 2$.

4.1. Deterministic case: family condensation and family demixing

In the deterministic case $\mathbf{C} = \mathbf{0}$, we recover an effective model describing a fluid of F components, corresponding to the F families, and with a virial matrix \mathbf{B}_{det} with entries $[\mathbf{B}_{\text{det}}]_{st} = c_t \mu_{st}$, where c_t is the fraction of species belonging to each family and $s, t \in \{1, 2, \dots, F\}$. Indeed, the spectrum of the matrix \mathbf{B} consists of two parts (see figure 1(a)): (i) a zero eigenvalue with multiplicity equal to $N - F$; (ii) F nonzero eigenvalues $\lambda_{\text{isol}} = \gamma_{\text{isol}} N$, where γ_{isol} are the eigenvalues of \mathbf{B}_{det} . Also the eigenvectors of \mathbf{B} are determined by \mathbf{B}_{det} : the F eigenvectors associated with the F isolated eigenvalues λ_{isol} have components v_i that depend only on the family to which the species i belongs, i.e., $v_i = V_{s(i)}$. The variables V_s are the eigenvector components of \mathbf{B}_{det} associated with the eigenvalues γ_{isol} :

$$V_s = \frac{1}{\gamma_{\text{isol}}} \sum_{t=1}^F c_t \mu_{st} V_t. \quad (5)$$

Let us now discuss the consequences of the spectrum of \mathbf{B} on phase separation. The smallest eigenvalue of \mathbf{B} is either 0 or the minimum λ_{isol}^- of the F non trivial eigenvalues. In the former case, the critical density (2) is infinite and therefore the homogeneous phase $\vec{\rho}_0$ is always stable. In the latter case, ρ_c is of order $\mathcal{O}(1)$ for large N as λ_{isol}^- scales linearly with N .

The nature of the liquid instability is determined by the V_1, \dots, V_F that solve (5). For $F = 1$ the only possible unstable mode is parallel to $\vec{\rho}_0$ and we recover the condensation instability of [5]. For a generic F , the possibilities are much richer and it is useful to distinguish two cases. When all V_s have the same sign, then one of the daughter phases is enriched in all species, albeit in proportions depending on their family. We refer to this kind of instability as *family condensation* and θ is geometrically bounded $0 \leq \theta \leq \arccos(\sqrt{c_{\text{min}}})$, where $c_{\text{min}} = \min_s c_s$. Conversely, when not all V_s have the same sign, one daughter phase is enriched in some species and deprived in others, depending on which family they belong to. We refer to this kind of instabilities as *family demixing* and θ is geometrically bounded $\arccos(\sqrt{c_{\text{max}}}) \leq \theta \leq \pi/2$, where $c_{\text{max}} = \max_s c_s$. In the latter case, there exists a region in the space of parameters for which $\theta = \pi/2$, corresponding to a demixing instability at finite critical density.

In the next sections we show that this picture is robust against the addition of disorder to the virial matrix.

4.2. Uniform noise amplitude

We now add uniform noise to the matrix of virial coefficients so that $\mathbf{C} = \sigma \mathbf{1}$. This case is analytically solvable as it corresponds to a finite rank perturbation of a Wigner

random matrix \mathbf{Z} [31]. As illustrated in figure 1(b), the main effect of the noise is the appearance of a continuous spectrum described by the Wigner's semicircle law supported on the interval $[-2\sigma\sqrt{N}, 2\sigma\sqrt{N}]$ [19, 32, 33]. On the other hand, the spectrum of \mathbf{B} retains the eigenvalues of the deterministic matrix \mathbf{D} , and at finite but large N these are located at $\lambda_{\text{isol}} = N\gamma_{\text{isol}} + \sigma^2/(N\gamma_{\text{isol}})$, where γ_{isol} are as before the eigenvalues of \mathbf{B}_{det} . Consequently, the critical density

$$\rho_c = \min \left\{ \frac{\sqrt{N}}{2\sigma}, -\frac{\gamma_{\text{isol}}^-}{(\gamma_{\text{isol}}^-)^2 + \sigma^2/N} \right\} \quad (6)$$

corresponds to a minimal eigenvalue λ_- equal to either the lower edge of the continuous spectrum or the smallest outlier, respectively. In the former case, ρ_c scales as \sqrt{N} and the associated eigenvector is a random vector with Gaussian components. Such an eigenvector describes a demixing phase transition referred to as *random demixing* [5]. In the latter case, ρ_c and its associated eigenvector both converge for large N to the corresponding quantities in the deterministic model and thus describe a transition to a family condensation or family demixing phase. Note that at finite values of N , the crossover between random demixing and family condensation (or family demixing) happens at $\sigma^* \approx \sqrt{N}\gamma_{\text{isol}}^-$.

4.3. General case

In the general case where noise amplitudes are not uniform, the picture is qualitatively equivalent to that of the perturbed Wigner case. If λ_- is located at the edge of the continuous spectrum, then the fluid is unstable w.r.t. random demixing at $\rho_c \sim \sqrt{N}$. On the other hand, if λ_- is an outlier, then the fluid is unstable w.r.t. family condensation or family demixing at $\rho_c \sim \mathcal{O}(1)$.

Quantitatively the critical density ρ_c is different from its value at uniform amplitudes. Indeed, the entries $v_i = V_{s(i)}$ of eigenvectors associated with outlier eigenvalues solve [34–37] (see also Appendix A)

$$V_s = G_s(\lambda) \sum_{t=1}^F c_t \mu_{st} V_t, \quad s \in \{1, \dots, F\}, \quad (7)$$

where $G_s(\lambda)$ satisfy

$$\frac{1}{G_s} = \lambda - \sum_{t=1}^F c_t \sigma_{st}^2 G_t, \quad s \in \{1, \dots, F\} \quad (8)$$

and are the diagonal components of the resolvent $G_B = (z\mathbb{1} - \mathbf{B})^{-1}$ [37, 38]. The linear system (7) has a non-zero solution when λ_{isol} is an outlier of \mathbf{B} [39]. Note that in the case of uniform noise, (7) reduces to (5).

The continuous part of the spectrum is not a Wigner semicircle can be computed from (8) and (A.10) and (A.16) in the Appendix A.4. We show an example of a continuous spectrum that is not a semicircle in figure 1(c). The eigenvectors associated

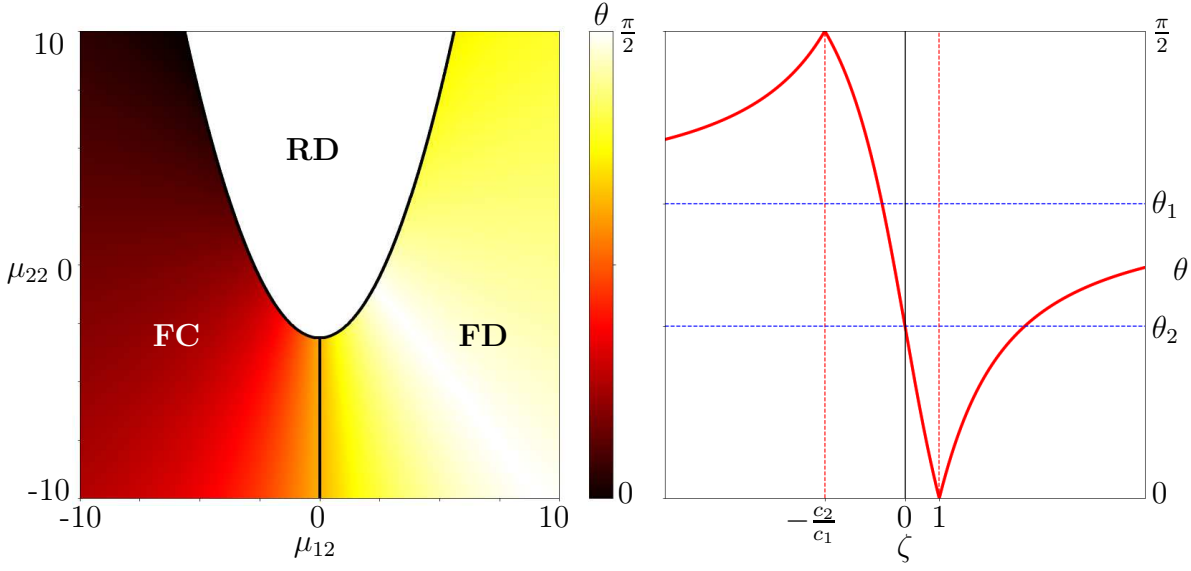


Figure 3. Demixing angle θ characterising the instability of a complex fluid. Parameters are set as in figure 2. On the left, a heatmap of θ : in the **FC** region, $\zeta > 0$ and $\theta < \theta_1 = \arccos(\sqrt{c_1})$; in the **FD** region $\zeta < 0$ and $\theta > \theta_2 = \arccos(\sqrt{c_2})$; in the **RD** region $\theta = \pi/2$. On the right, θ as a function of ζ for $c_1 = 0.3$. Extremes (red) and asymptotes (blue) are highlighted by dashed lines.

with eigenvalues at the edge of the continuous spectrum are random vectors with entries v_i that are drawn independently from Gaussian distributions with zero mean and with variances $\Delta_{s(i)}$ that depend on the family $s(i)$ that the i -th index belongs to. As shown in Appendix A.4, the variances Δ_s solve the equations

$$\Delta_s = G_s^2(\lambda) \sum_{t=1}^F c_t \sigma_{st}^2 \Delta_t. \quad (9)$$

In the case of uniform noise amplitudes $\sigma_{st} = \sigma$, we obtain that $\Delta_s = \Delta$ and thus we recover the results from the previous section.

5. Spinodals for two families ($F = 2$)

We now illustrate the influence of randomness on fluid instabilities in the case of two families $F = 2$. Figure 2 shows the critical density ρ_c as a function of two system parameters for fluid instabilities towards the family condensation, family demixing, and random demixing phases. The deterministic case figure 2(a) has a stable region that is destabilised by random demixing with the addition of noise figure 2(b). Note that figure 2(b) is in the cross-over regime where the variances of the virial coefficients scale linearly with N , so the boundary between random demixing and other types of instabilities gets a contribution from noise terms as well.

Provided that λ_- is an outlier, v^- can be cast in the form $(\zeta, \dots, \zeta, 1, \dots, 1)$ with $\zeta = V_1/V_2$ (see Appendix B). This form of the unstable mode forces the local demixing

angle to be

$$\theta = \min\{\tilde{\theta}, \pi - \tilde{\theta}\}, \quad \tilde{\theta} = \arccos\left(\frac{c_1\zeta + c_2}{\sqrt{c_1\zeta^2 + c_2}}\right). \quad (10)$$

Expression (10) is of geometric nature, while ζ depends on the actual matrix model. We show a plot of θ as a function of ζ (see figure 3). The sign of ζ has a profound effect on the range of values that θ can take, as previously discussed. Interestingly, in all models we see that the only parameter influencing the sign of ζ is the interfamily average virial coefficient μ_{12} : $\text{sgn}(\zeta) = -\text{sgn}(\mu_{12})$. The physical picture is as follows: $\mu_{12} < 0$ if attractive interactions between the two families are dominant, so there is a net free energy gain if species of family 1 and 2 aggregate together; conversely, $\mu_{12} > 0$ when repulsive interactions between the two families are dominant, so there is a net free energy gain if the 2 families demix. In figure 3 we show a heatmap of θ for $F = 2$.

Pure condensation ($\theta = 0$) and pure demixing ($\theta = \pi/2$) occur respectively for $\zeta = 1$ and $\zeta = -c_2/c_1$. In the deterministic and uniform noise models, ζ is either 1 or $-c_2/c_1$ when there is a balance between interactions involving the 2 families: $\mu_{11}c_1 + \mu_{12}c_2 = \mu_{12}c_1 + \mu_{22}c_2$. In the general case, the non-uniformity of noises deforms this simple condition.

6. pH-induced phase transitions in the cytoplasm

It was shown in experiments that the cytoplasm of eukaryotic cells can undergo phase separation triggered by a change in pH [40, 41]. In what follows we use the model introduced in this paper to describe the instability of the homogeneous state of the cytoplasm at low pH values.

Proteins' interactions in solution depend on their isoelectric point (PI), defined as the pH at which the protein has no net charge. According to DLVO theory, at a pH significantly different from its PI a protein's net charge is screened by a double layer of ions [44, 45]. This phenomenon reduces the tendency to aggregate. Conversely, at a pH close to their PI proteins are more likely to aggregate [46].

An evolutionary conserved feature of distribution of PI across the proteome is its bimodality [47]. The bimodality of the PI distribution provides a natural way to split proteins into 2 families, one of acidic and one of basic species. The virial matrix should thus have a 2×2 block structure.

It is challenging to measure experimentally all the entries of the matrix of virial coefficients \mathbf{B} . At the moment only limited information is available in the literature [48–50]. This motivated us to examine a simple random model for the dependence of intra-family virial coefficients on the solvent's pH. We consider a Taylor expansion around the average isoelectric point plus noise, viz.

$$B_{ij}(x) = k(x - y_s)^2 + q + \xi_{ij}, \quad \text{if } s(i) = s(j) = s \in \{1, 2\}, \quad (11)$$

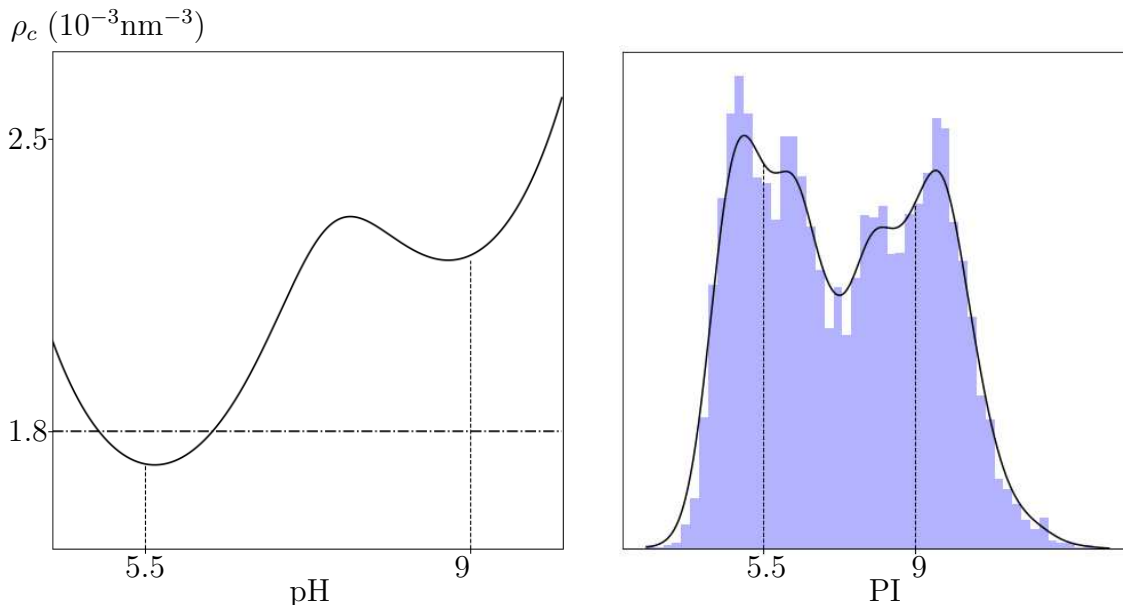


Figure 4. Left: the spinodal density ρ_c as a function of pH for the model (11) with parameters as described in Appendix C. The dash-dot line is a value $\rho^* = 1.8 \times 10^{-3} \text{nm}^{-3}$ compatible with experiments of the density of proteins in the cytosol [42]. We choose $c_1 = 0.55$ as the acidic family is more populated in living organisms. On the right, distribution of isoelectric points (PI) across the proteome of budding yeast (*Saccharomyces cerevisiae*). Data from [43].

where x is the solution pH, y_s is the average PI in family s , k and q are expansion coefficients, and ξ_{ij} are random variables with zero mean.

According to the double layer picture of proteins in solution, for two proteins with considerably different PI there is no pH at which the double layer is absent for both. This implies that short range attractive interactions contribute less to the inter-family virial coefficients, which is in agreement with experiments [50]. Therefore, for simplicity we model the inter-family virial coefficients B_{ij} with $s(i) \neq s(j)$ as a pH-independent constant μ_{12} plus noise ξ_{ij} , with $s(i) \neq s(j)$. Furthermore, we set the variances of both inter- and intra-family noises ξ_{ij} to be uniform and equal to σ^2 .

Figure 4 shows the critical density for family condensation and family demixing as a function of pH for the model (11) with parameters as described in Appendix C. We observe three interesting features: i) the order of magnitude of the critical density is close to the protein density in living cells; ii) the non-monotonicity of ρ_c entails the possibility of a re-entrant behavior, as highlighted in [51]; iii) an asymmetry in family sizes ($c_1 \neq 0.5$) leads to an asymmetry of the critical density w.r.t. the neutral pH. On one hand this strengthens the idea that pH can be used by living organisms as a control parameter for phase separation, while on the other hand it shows that these simple models are a promising tool to interpret biological data.

To investigate the relevance of random demixing, we assume that σ^2 is due to fluctuations of volume and that the number of proteins species in the cytosol is $\sim 10^4$ [42]. From (6) we obtain a critical density $\rho_c \sim \mathcal{O}(1 \text{ nm}^{-3})$ (see Appendix C), three

orders of magnitude higher than proteins concentration in the cytoplasm [42]. This suggests that a random demixing instability due to fluctuations in excluded volume is likely not to occur in living cells.

7. Conclusions

We determined how randomness and structure in the matrix of virial coefficients affects the instability of complex fluids. In contrast with fully random models, partially random models can describe demixing of complex fluids at a critical density that does not scale with N , which is in accordance with experimental findings in cell biology. Using the present framework it is possible to analyse how complexity in the number of components of a fluid affects phase separation and how to apply random matrix methods in existing models of phase separation of the cytosol, e.g. those in [51, 52], by describing the known parts of the interaction matrix with the deterministic matrix \mathbf{B}_{det} and the unknown parts of the system with noise dressing the entries of \mathbf{B} . Taken together, the theory of partially structured and partially random matrices provides a versatile tool for understanding the behavior of complex fluids.

Acknowledgments

GC would like to thank Francesco Coghi and Gianmichele Di Matteo for insightful discussions. IN thanks Omar Adame-Arana and Pablo Sartori for fruitful discussions. GC is supported by the EPSRC Centre for Doctoral Training in Cross-Disciplinary Approaches to Non-Equilibrium Systems (CANES, EP/L015854/1).

Appendix A. Spectrum of block matrices

Let \mathbf{B} be a symmetric $N \times N$ random matrix with a $F \times F$ block structure in the following sense: the entries B_{ij} are independent random variables with finite means $\langle B_{ij} \rangle = \mu_{s(i)s(j)}$ and variances $\text{Var}(B_{ij}) = \sigma_{s(i)s(j)}^2$, where the function $s(i)$ returns the family $s \in \{1, \dots, F\}$ to which the i -th index belongs.

In this appendix, we derive a set of equations that determine the empirical spectral density of \mathbf{B} , the eigenvalue outliers, and the moments of the eigenvectors associated with either the outlier eigenvalues or the eigenvalues at the edge of the spectral density.

It is convenient to consider a rescaled version of \mathbf{B} , which we will call $\tilde{\mathbf{B}}$, whose entries have means $\langle \tilde{B}_{ij} \rangle = \mu_{s(i)s(j)}/N$ and variances $\text{Var}(\tilde{B}_{ij}) = \sigma_{s(i)s(j)}^2/N$. This choice is such that both outliers and the support of the spectral density $\nu(\lambda)$ of $\tilde{\mathbf{B}}$ are of order

$\mathcal{O}(1)$ for large N , and they are connected to those of \mathbf{B} as follows:

$$\nu_B(\lambda) = \nu_{\tilde{B}}(\lambda/\sqrt{N}) \quad (\text{A.1})$$

$$\lambda_{\text{isol}}(B) (\boldsymbol{\mu}, \boldsymbol{\Sigma}) = \lambda_{\text{isol}}(\tilde{B}) (N\boldsymbol{\mu}, N\boldsymbol{\Sigma}), \quad (\text{A.2})$$

where $\boldsymbol{\mu}$ and $\boldsymbol{\Sigma}$ are $F \times F$ symmetric matrices containing the means μ_{st} and the variances σ_{st}^2 .

Appendix A.1. A reminder of some equalities for block matrices

In this section, we review a few equalities for the inverse and the determinant of a block matrix. Let \mathbf{M} be a $N \times N$ block matrix, then the Schur formula states [53]

$$\mathbf{M} = \left(\begin{array}{c|c} \mathbf{a} & \mathbf{b} \\ \hline \mathbf{c} & \mathbf{d} \end{array} \right). \quad (\text{A.3})$$

The Schur formula for the inverse of \mathbf{M} is

$$\mathbf{M}^{-1} = \left(\begin{array}{c|c} \mathbf{s}_d^{-1} & -\mathbf{s}_d^{-1}\mathbf{b}\mathbf{d}^{-1} \\ \hline -\mathbf{d}^{-1}\mathbf{c}\mathbf{s}_d^{-1} & \mathbf{s}_a^{-1} \end{array} \right), \quad (\text{A.4})$$

where

$$\mathbf{s}_a = \mathbf{d} - \mathbf{c}\mathbf{a}^{-1}\mathbf{b}, \quad (\text{A.5})$$

and

$$\mathbf{s}_d = \mathbf{a} - \mathbf{b}\mathbf{d}^{-1}\mathbf{c}. \quad (\text{A.6})$$

We will also use the formula

$$\det(\mathbf{M}) = \det(\mathbf{a} - \mathbf{b}\mathbf{d}^{-1}\mathbf{c}) \det(\mathbf{d}) \quad (\text{A.7})$$

for the determinant of a block matrix.

Appendix A.2. The resolvent

A standard approach in random matrix theory to analyse the spectrum of a large random matrix is based on the resolvent $G(z)$ defined as

$$G(z) = \frac{1}{\mathbb{1}z - \mathbf{B}}, \quad (\text{A.8})$$

for all values $z \in \mathbb{C} / \{\lambda_1, \lambda_2, \dots, \lambda_N\}$, and where $\mathbb{1}$ is the identity matrix of size N . If we know the trace resolvent

$$\mathcal{G}(z) = \lim_{N \rightarrow \infty} \frac{1}{N} \mathbb{E} [\text{Tr}G(z)], \quad (\text{A.9})$$

then the spectral density follows readily from [53]

$$\nu(\lambda) = \lim_{\epsilon \rightarrow 0} \frac{1}{\pi} \text{Im} \mathcal{G}(\lambda - i\epsilon). \quad (\text{A.10})$$

As shown in [32, 53], the trace resolvent $\mathcal{G}(z)$ of a random matrix can be determined from the Schur formula (A.4). In what follows we use this method to determine the trace resolvent of the block matrix \mathbf{B} .

Let us represent $\mathbb{1}z - \tilde{\mathbf{B}}$ as a 2×2 block matrix

$$\mathbb{1}z - \tilde{\mathbf{B}} = \left(\begin{array}{c|c} z - \tilde{B}_{11} & \tilde{\mathbf{B}}_1 \\ \hline \tilde{\mathbf{B}}_1^T & (\mathbb{1}z - \tilde{\mathbf{B}})^{(1)} \end{array} \right), \quad (\text{A.11})$$

where $\tilde{\mathbf{B}}_1$ is the $(N-1)$ -dimensional vector of components \tilde{B}_{1j} with $j \neq 1$. We use $M^{(i)}$ to denote the $(N-1) \times (N-1)$ principal submatrix obtained from M by eliminating the i -th row and i -th column. Applying the Schur formula to $(\mathbb{1}z - \tilde{\mathbf{B}})^{-1}$, we can express the diagonal $(1, 1)$ -element as

$$\frac{1}{G_{11}} = z - \tilde{B}_{11} - \sum_{j=1}^N \sum_{k=2}^N \tilde{B}_{1j} G_{jk}^{(1)} \tilde{B}_{k1}, \quad (\text{A.12})$$

where we used $G^{(1)} = 1/(\mathbb{1}z - \tilde{\mathbf{B}}^{(1)})$. Swapping the first vector of the basis with the i -th vector and then applying the Schur formula as above gives an expression similar to (A.12) where index 1 is replaced by index i , viz.,

$$\frac{1}{G_{ii}} = z - \tilde{B}_{ii} - \sum_{j=1}^N \sum_{k=1(k \neq i)}^N \tilde{B}_{ij} G_{jk}^{(i)} \tilde{B}_{ki}. \quad (\text{A.13})$$

For large values of N , we can neglect the \tilde{B}_{ii} term in (A.13) as it scales as $\mathcal{O}(1/N)$ with the system size. In addition, in the Appendix A.3 we show that the scaling of the off-diagonal elements of the resolvent with respect of N is subleading with respect to the scaling of the diagonal elements, and therefore

$$\frac{1}{G_{ii}} = z - \sum_{j=1(j \neq i)}^N \tilde{B}_{ij}^2 G_{jj}^{(i)}. \quad (\text{A.14})$$

Because of the law of large numbers it holds that for large values of N the sum in the right-hand side of (A.14) is equal to its average value and therefore G_{ii} is a deterministic variable in the limit of N large. In particular, we find that G_{ii} only depends on the family $s(i)$ to which the index i belongs, allowing us to make the simplification $G_{ii} = G_{s(i)}$. In addition to that, using that $G_{jj}^{(i)} = G_{jj}(1 + \mathcal{O}(1/N)) = G_{s(j)}(1 + \mathcal{O}(1/N))$, we arrive at

$$\frac{1}{G_s} = z - \sum_{t=1}^F c_t \sigma_{st}^2 G_t, \quad (\text{A.15})$$

with $c_t = \lim_{N \rightarrow \infty} N_t/N$, which is also (8) in the main text. Solving the set of F equations (A.15) towards the F variables G_s , one obtains for large N the trace resolvent

$$\mathcal{G} = \sum_{t=1}^F c_t G_t, \quad (\text{A.16})$$

and thus also the spectral density through (A.10).

Appendix A.3. Off-diagonal elements of the resolvent

In this section we show that the off-diagonal elements G_{ij} with $i \neq j$ scale as $1/N$. In particular, we show that both the first and second moments of G_{ij} scale as $1/N$.

We start from the adjugate representation of the inverse of a matrix to express G_{ij} as

$$G_{ij} = \frac{\det(z\mathbb{1} - \tilde{\mathbf{B}}^{(i,j)})}{\det(z\mathbb{1} - \tilde{\mathbf{B}})}, \quad (\text{A.17})$$

where $\tilde{\mathbf{B}}^{(i,j)}$ is obtained from $\tilde{\mathbf{B}}$ by removing the i -th row and the j -th column. Using the formula (A.7) for the determinant of a block matrix we obtain

$$G_{ij} = \frac{-\tilde{B}_{ij} - \sum_{k,l(\neq i,j)}^N \tilde{B}_{ik} G_{kl}^{(i)(j)} \tilde{B}_{jl}}{\left[z - \tilde{B}_{ii} - \sum_{k,l(\neq i,j)}^N \tilde{B}_{ik} G_{kl}^{(i)(j)} \tilde{B}_{il} \right] \left[z - \tilde{B}_{jj} - \sum_{k,l(\neq i,j)}^N \tilde{B}_{jk} G_{kl}^{(i)(j)} \tilde{B}_{jl} \right] - \left[\sum_{k,l(\neq i,j)}^N \tilde{B}_{ik} G_{kl}^{(i)(j)} \tilde{B}_{jl} \right]^2}, \quad (\text{A.18})$$

where $G^{(i)(j)}$ denotes the resolvent of the matrix $\mathbf{B}^{(i)(j)}$ obtained from \mathbf{B} by removing the i -th row and column and the j -th row and column. For large N , we have that $G_{kl}^{(i)(j)} = G_{kl}(1 + O(1/N))$.

Suppose now that the average of G_{kl} scales as $N^{-\delta_1}$ and its variance scales as $N^{-\delta_2}$, where $\delta_1, \delta_2 \in \mathbb{R}$. Equation (A.18) provides us with a self-consistent equation for the exponents δ_1 and δ_2 . Solving this equation we find that $\delta_1 = \delta_2 = 1$. This implies that the average value and the variance of G_{ij} are both of the order $O(1/N)$.

We remark that analogous arguments hold also for the resolvent $G^{(i)}$ of the matrix $\mathbf{B}^{(i)}$, in particular $G_{jk}^{(i)}$ is negligible for large N w.r.t the diagonal elements $G_{jj}^{(i)}$.

Appendix A.4. Outlier eigenvalues and the components of eigenvectors

We derive a set of equations solved by the entries v_i of eigenvectors associated with either eigenvalue outliers or eigenvalues located at the boundary of the continuous part of the spectrum of block matrices. The general approach we follow is based on [37] that deals with sparse random matrices, but as we will see, dealing with dense matrices has some advantages and lead to some analytical simplifications.

First we establish a connection between the eigenvector components and the off-diagonal elements of the resolvent $G(z)$. Let λ be an eigenvalue of $\tilde{\mathbf{B}}$ with an algebraic multiplicity equal to 1, then the resolvent $G(z)$ has a simple pole at λ and [37]

$$\lim_{\eta \rightarrow 0} \eta G(\lambda - \eta) = \vec{v} \vec{v}^T, \quad (\text{A.19})$$

where η is a small complex number and \vec{v} is the normalised eigenvector associated with λ . It follows from (A.19) that the i -th component of \vec{v} is given by

$$v_i = \lim_{\eta \rightarrow 0} \eta \frac{\sum_{j=1}^N G_{ij}(\lambda - \eta)}{\vec{v} \cdot \vec{1}}, \quad (\text{A.20})$$

where we have used $\vec{1}$ for the vector with all components equal to 1. Equation (A.20) links the components of eigenvectors to the off-diagonal entries of the resolvent.

Note that the parameter η in (A.19)-(A.20) has to be much smaller than the separation between eigenvalues. Therefore, in the limit of $N \gg 1$, (A.19)-(A.20) are only useful for eigenvalue outliers or eigenvalues at the edge of the continuous spectrum.

The off-diagonal entries of the resolvent solve a set of self-consistent equations that we derive now. Applying the Schur formula to the resolvent $G(z)$, we obtain

$$G_{ij} = G_{ii} \sum_{k=1(k \neq i)}^N \tilde{B}_{ik} G_{kj}^{(i)}, \quad (\text{A.21})$$

where we mean again by $G^{(i)}$ the principal submatrix of G obtained by removing the i -th row and the i -th column. Summing over index j we obtain

$$\sum_{j=1}^N G_{ij} = G_{ii} \left(1 + \sum_{j=1}^N \sum_{k=1(k \neq i)}^N \tilde{B}_{ik} G_{kj}^{(i)} \right), \quad (\text{A.22})$$

and consequently substituting (A.22) in (A.20) we get

$$v_i = \lim_{\eta \rightarrow 0} \eta \frac{G_{ii}(\lambda - \eta)}{\vec{v} \cdot \vec{1}} + G_{ii} \sum_{k=1(k \neq i)}^N \tilde{B}_{ik} \lim_{\eta \rightarrow 0} \eta \frac{\sum_{j=1(j \neq i)}^N G_{kj}^{(i)}(\lambda - \eta)}{\vec{v} \cdot \vec{1}}. \quad (\text{A.23})$$

The first term converges to zero for large N and

$$v_k^{(i)} = \lim_{\eta \rightarrow 0} \eta \frac{\sum_{j=1(j \neq i)}^N G_{kj}^{(i)}(\lambda - \eta)}{\vec{v}^{(i)} \cdot \vec{1}} \approx \lim_{\eta \rightarrow 0} \eta \frac{\sum_{j=1(j \neq i)}^N G_{kj}^{(i)}(\lambda - \eta)}{\vec{v} \cdot \vec{1}} \quad (\text{A.24})$$

is identified as the k -th element of the eigenvector associated with λ of the submatrix $\tilde{\mathbf{B}}^{(i)}$. This identification is consistent only if λ is an eigenvalue of both $\tilde{\mathbf{B}}$ and $\tilde{\mathbf{B}}^{(i)}$, which applies for eigenvalue outliers and the edge of the spectral density when N is large. In the last passage of (A.24) we have used the law of large numbers to identify $\vec{v}^{(i)} \cdot \vec{1}$ with $\vec{v} \cdot \vec{1}$. From (A.24) it follows that we can express v_i in terms of $v_k^{(i)}$, viz.,

$$v_i = \lim_{\eta \rightarrow 0} G_{ii}(\lambda - \eta) \sum_{k=1(k \neq i)}^N \tilde{B}_{ik} v_k^{(i)} \quad (\text{A.25})$$

The difference between v_k and $v_k^{(i)}$ decreases when N increases, as can be seen from comparing (A.20) with (A.24) and noting that the law of large numbers holds for both the numerators and the denominators. With the relabelling $k \rightarrow j$, we arrive at

$$v_i = \lim_{\eta \rightarrow 0} G_{ii}(\lambda - \eta) \sum_{j=1(j \neq i)}^N \tilde{B}_{ij} v_j. \quad (\text{A.26})$$

We remark that (A.26) applies to the entries v_i of eigenvectors associated with eigenvalue outliers $\lambda = \lambda_{\text{isol}}$ and eigenvectors associated with eigenvalues λ located at the edge of the continuous spectrum.

If $\lambda = \lambda_{\text{isol}}$, then the expected values $\langle v_j \rangle \neq 0$. Therefore, we can apply the law of large numbers to (A.26) to get $v_i = V_{s(i)}$, where the V_s are deterministic variables that

solve (7). One can verify that (7) only admits a nontrivial solution, i.e. $V_s \neq 0$, when $\lambda = \lambda_{\text{isol}}$. Hence, the locations of the eigenvalue outliers can be obtained by setting the determinant of the linear system (7) equal to zero.

If λ is set equal to one of the edges of the continuous spectrum, then the means of v_i are equal to zero. In this case the central limit theorem applies and consequently the v_i are Gaussian random variables with zero mean and variance $\Delta_{s(i)}$ that only depend on the family to which the index i belongs. From (A.26) it follows that the variances solve (9). Also, the edge of the spectrum can be obtained by finding the values of λ for which (9) admit a nontrivial solution. For this, one can again find the values of λ for which the determinant of the linear system, in this case given by (9), is equal to zero.

Appendix B. Unstable mode due to outliers for $F = 2$

In this appendix we characterise explicitly the unstable mode of a complex fluid composed of 2 families of interacting species. We consider three cases depending on the assumptions made on the interaction matrix \mathbf{B} : i) deterministic interactions; ii) random interactions with uniform variances; iii) random interactions with family-dependent variances. Note that these are also the three cases illustrated in figure 1.

We focus on fluid instabilities that are governed by an isolated eigenvalue λ_{isol} . Since eigenvectors are defined up to a proportional constant, we can, for values $V_2 \neq 0$, cast the unstable mode into the form $v^- = (\zeta, \dots, \zeta, 1, \dots, 1)$, where $\zeta = V_1/V_2$. In what follows we determine ζ as a function of the system parameters.

Appendix B.1. Deterministic case

When interactions are deterministic, a complex fluid composed by $F = 2$ families is unstable when the lowest of the two non-zero eigenvalues of \mathbf{B} are negative. We get for ζ the expression

$$\zeta = \frac{\mu_{11}c_1 - \mu_{22}c_2}{2\mu_{12}c_1} - \frac{\sqrt{(\mu_{11}c_1 - \mu_{22}c_2)^2 + 4c_1c_2\mu_{12}^2}}{2\mu_{12}c_1}. \quad (\text{B.1})$$

Remarkably, the sign of ζ depends only on the sign of μ_{12} , i.e., $\text{sgn}(\zeta) = -\text{sgn}(\mu_{12})$.

Appendix B.2. Uniform noise

When interactions are noisy, the instability is either due to the lower edge of the continuous part of the spectrum or due to one of the outliers. When noises are uniform, the latter case is particularly simple. In fact, the solubility condition of (7) is

$$\mathcal{G}(\lambda_{\text{isol}}) = \frac{1}{\gamma_{\text{isol}}}. \quad (\text{B.2})$$

Substituting (B.2) back into (7) we obtain that V_1 and V_2 solve the same equations as those solved by the corresponding eigenvalue in the deterministic case and therefore ζ is also given by (B.1).

Appendix B.3. Family-dependent noise

Contrary to the uniform case, when the noise in the virial matrix is family dependent and the instability is due to an outlier λ_{isol} , the unstable mode depends also on the variances of the noise. When $F = 2$, we can express ζ from (7) as

$$\zeta = \frac{G_1(\lambda_{\text{isol}})c_2\mu_{12}}{1 - G_1(\lambda_{\text{isol}})c_1\mu_{11}}. \quad (\text{B.3})$$

From (A.15), one can prove that $G_1(z)$ solves a quartic equation

$$\begin{aligned} & \sigma_{11}^2 c_1^2 (\sigma_{12}^4 - \sigma_{11}^2 \sigma_{22}^2) G_1^4(z) + c_1 (2\sigma_{11}^2 \sigma_{22}^2 - \sigma_{11}^2 \sigma_{12}^2 - \sigma_{12}^4) z G_1^3(z) + \\ & + [z^2 (\sigma_{12}^2 - \sigma_{22}^2) + (c_1 - c_2) \sigma_{12}^4 - 2c_1 \sigma_{11}^2 \sigma_{22}^2] G_1^2(z) + (2\sigma_{22}^2 - \sigma_{12}^2) z G_1(z) - \sigma_{22}^2 = 0. \end{aligned} \quad (\text{B.4})$$

Numerical calculations show that if λ_{isol} is the lowest outlier of $\tilde{\mathbf{B}}$, the sign of ζ depends only on the sign of μ_{12} as in previous cases: $\text{sign}(\zeta) = -\text{sign}(\mu_{12})$.

Appendix C. Parameters used for the model of pH-induced phase transitions in the cytosol used in figure 4

We first discuss the parameters used in figure 4 for the model for pH induced phase transitions in the cytosol described in section 6, and second, we estimate the critical density at which volume fluctuations destabilise a fluid of hard spheres.

Appendix C.1. Estimated parameters for the cytosol

Reference [43] contains the isoelectric points of the proteomes of several organisms, among which humans and budding yeast. For example, in figure 4 we have plotted the distribution of isoelectric points in the latter. Since the distribution is bimodal, we can use the two peak values of the distribution to estimate the average PI in each family. For budding yeast this gives us $y_1 = 5.5$ and $y_2 = 9$. Furthermore, from figure 4 we estimate the fraction of species in the acidic family to be $c_1 = 0.55$.

In [48,49] the virial coefficients of some proteins have been measured experimentally. From their results, we identify a plausible physical range of the average intra-family virial coefficients between -10^3 nm^3 and $+10^3 \text{ nm}^3$. To reproduce this range of values, in the model given by (11) we set the parameter values $k = 10^2 \text{ nm}^3$ and $q = -10^3 \text{ nm}^3$. Experimental results of [50] indicate that on average the cross virial coefficients are one order of magnitude less than the intra-species virial coefficients, and therefore we set $\mu_{12} = \pm 250 \text{ nm}^3$.

By assuming that proteins are hard spheres, the variance σ^2 of the noise variables can be estimated from the fluctuations in the protein volumes. Indeed, for hard spheres an explicit expression for B_{ij} is known. If species i and j have radii r_i and r_j , respectively, then [54]:

$$B_{ij} = \frac{2}{3}(r_i + r_j)^3. \quad (\text{C.1})$$

In particular, when $i = j$, then $B_{ii} = 4V$, where V is the volume of a sphere of radius r_i . Hence, fluctuations in the volumes of hard spheres lead to fluctuations in the virial coefficients B_{ij} , and we can estimate the standard deviation σ of B_{ij} from the variance σ_V of the protein volume V with the formula

$$\sigma = 4 \sigma_V . \quad (\text{C.2})$$

To estimate the variance σ_V^2 of the volume fluctuations of proteins, we start from the distribution of the number of aminoacids in proteins. The standard deviation of this distribution is of the order $\sim 10^2$ [42]. Since the weighted average of aminoacids' mass is ~ 110 Da, where $1 \text{ Da} = 1 \text{ g/1 mol}$, the standard deviation in protein mass is of the order 10^4 Da. For folded proteins, we have that [55]

$$V(\text{nm}^3) = \frac{1}{\phi_p} \times M(\text{Da}) . \quad (\text{C.3})$$

where

$$\phi_p = 0.825 \left(\frac{\text{Da}}{\text{nm}^3} \right) \quad (\text{C.4})$$

is the average density of a protein. This phenomenological relation gives a standard deviation for the volume of the order $\sigma_V \sim 10 - 10^2 \text{ nm}^3$ and thus from (C.2) $\sigma \sim 10 - 10^3 \text{ nm}^3$. To generate the plot in figure 4, we have used $\sigma = 100 \text{ nm}^3$.

Appendix C.2. Critical spinodal density ρ_c for a complex fluid of hard spheres

We can estimate the number of proteins species in a cell to be approximately the number of protein coding genes, which is $N \sim 10^4$ [42]. Recalling that for random demixing $\rho_c = \sqrt{N}/\sigma$, we get the estimate $\rho_c \sim 10^0 \text{ nm}^3$. Since for living cells $\rho^* \sim 10^{-3} \text{ nm}^{-3}$ [42], this suggests that random demixing due to fluctuations in volume is not likely to happen in living organisms.

References

- [1] C. P. Brangwynne, C. R. Eckmann, C. D. S. A. Rybarska, C. Hoegel, J. Gharakhani, F. Jülicher, and A. A. Hyman, "Germline P-granules are liquid droplets that localize by controlled dissolution/condensation.," *Science*, vol. 324(5935), p. 1729:1732, jun 2009.
- [2] A. A. Hyman, C. A. Weber, and F. Jülicher, "Liquid-Liquid Phase Separation in Biology," *Annu. Rev. Cell Dev. Biol.*, vol. 30, p. 39:58, 2014.
- [3] R. P. Sear, "The cytoplasm of living cells: a functional mixture of thousands of components," *Journal of Physics: Condensed Matter*, vol. 17, p. S3587:S3595, oct 2005.
- [4] E. A. Ponomarenko, E. V. Poverennaya, E. V. Ilgisonis, M. A. Pyatnitskiy, A. T. Kopylov, V. G. Zgoda, A. G. Lisitsa, and A. I. Archakov, "The Size of the Human Proteome: The Width and Depth," *International journal of analytical chemistry*, vol. 7436849, 2016.
- [5] R. P. Sear and J. A. Cuesta, "Instabilities in complex mixtures with a large number of components," *Phys. Rev. Lett.*, vol. 91, p. 245701, Dec 2003.
- [6] W. M. Jacobs and D. Frenkel, "Predicting phase behavior in multicomponent mixtures," *The Journal of chemical physics*, vol. 139, no. 2, p. 24108, 2013.
- [7] W. M. Jacobs and D. Frenkel, "Phase Transitions in Biological Systems with Many Components," *Biophysical Journal*, vol. 112, no. 4, p. 683:691, 2017.

- [8] W. M. Jacobs, “Self-Assembly of Biomolecular Condensates with Shared Components,” *Phys. Rev. Lett.*, vol. 126, p. 258101, jun 2021.
- [9] K. Simons and J. L. Sampaio, “Membrane organization and lipid rafts,” *Cold Spring Harb Perspect Biol.*, vol. 3(10), p. a004697, 2011.
- [10] P. Sengupta, B. Baird, and D. Holowka, “Lipid rafts, fluid/fluid phase separation, and their relevance to plasma membrane structure and function,” *Seminars in Cell & Developmental Biology*, vol. 18, no. 5, p. 583:590, 2007.
- [11] T. Duke and I. Graham, “Equilibrium mechanisms of receptor clustering,” *Progress in Biophysics and Molecular Biology*, vol. 100, no. 1, p. 18:24, 2009.
- [12] P. Sartori and S. Leibler, “Lessons from equilibrium statistical physics regarding the assembly of protein complexes,” *Proceedings of the National Academy of Sciences*, vol. 117, no. 1, p. 114:120, 2020.
- [13] P. De Castro and P. Sollich, “Phase separation dynamics of polydisperse colloids: a mean-field lattice-gas theory,” *Phys. Chem. Chem. Phys.*, vol. 19, no. 33, p. 22509:22527, 2017.
- [14] P. De Castro and P. Sollich, “Phase separation of mixtures after a second quench: composition heterogeneities,” *Soft Matter*, vol. 15, no. 45, p. 9287:9299, 2019.
- [15] M. Fasolo and P. Sollich, “Fractionation effects in phase equilibria of polydisperse hard-sphere colloids,” *Phys. Rev. E*, vol. 70, p. 041410, oct 2004.
- [16] C. Noik and T. Palermo, “Modeling of Liquid/Liquid Phase Separation: Application to Petroleum Emulsions,” *Journal of Dispersion Science and Technology*, vol. 34(8), p. 1029:1042, 2013.
- [17] C.-E. Boukaré and Y. Ricard, “Modeling phase separation and phase change for magma ocean solidification dynamics,” *Geochemistry, Geophysics, Geosystems*, vol. 18, no. 9, p. 3385:3404, 2017.
- [18] E. P. Wigner, “On the statistical distribution of the widths and spacings of nuclear resonance levels,” in *Mathematical Proceedings of the Cambridge Philosophical Society*, vol. 47, p. 790:798, Cambridge University Press, 1951.
- [19] G. Livan, M. Novaes, and P. Vivo, “Introduction to Random Matrices: Theory and Practice,” *Springer*, 2017.
- [20] J. R. Espinosa, J. A. Joseph, I. Sanchez-Burgos, A. Garaizar, D. Frenkel, and R. Collepardo-Guevara, “Liquid network connectivity regulates the stability and composition of biomolecular condensates with many components,” *Proceedings of the National Academy of Sciences*, vol. 117, no. 24, p. 13238:13247, 2020.
- [21] W. G. McMillan and J. E. Mayer, “The Statistical Thermodynamics of Multicomponent Systems,” *The Journal of Chemical Physics*, vol. 13, no. 7, p. 276:305, 1945.
- [22] S. Vafaei, B. Tomberli, and C. G. Gray, “McMillan-Mayer theory of solutions revisited: Simplifications and extensions,” *The Journal of Chemical Physics*, vol. 141, no. 15, p. 154501, 2014.
- [23] L. D. Landau and E. M. Lifshitz, “Course on theoretical physics,” *Elsevier*, vol. 5, 1980.
- [24] H. B. Callen, “Thermodynamics and an Introduction to Thermostatistics,” *American Association of Physics Teachers*, 1998.
- [25] F. Zamponi, G. Parisi, and P. Urbani, “Theory of simple glasses,” *Cambridge University Press*, 2020.
- [26] P. Sollich, “Predicting phase equilibria in polydisperse systems,” *Journal of Physics: Condensed Matter*, vol. 14, p. R79–R117, Dec 2001.
- [27] R. M. May, “Will a large complex system be stable?,” *Nature*, vol. 238, no. 5364, p. 413:414, 1972.
- [28] L. Laloux, P. Cizeau, J.-P. Bouchaud, and M. Potters, “Noise dressing of financial correlation matrices,” *Physical Review Letters*, vol. 83, no. 7, p. 1467, 1999.
- [29] Y. Ahmadian, F. Fumarola, and K. D. Miller, “Properties of networks with partially structured and partially random connectivity,” *Physical Review E*, vol. 91, no. 1, p. 012820, 2015.
- [30] J. Aljadeff, D. Renfrew, M. Vegué and T.O. Sharpee, “Low-dimensional dynamics of structured random networks,” *Phys. Rev. E*, vol. 93, no. 1, p. 022302, 2016.

- [31] M. Capitaine, C. Donati-Martin, D. Féral, and Others, “The largest eigenvalues of finite rank deformation of large Wigner matrices: convergence and nonuniversality of the fluctuations,” *The Annals of Probability*, vol. 37, no. 1, p. 1:47, 2009.
- [32] M. Potters and J.-P. Bouchaud, “A First Course in Random Matrix Theory: for Physicists, Engineers and Data Scientists,” *Cambridge University Press*, 2020.
- [33] M. L. Mehta, “Random Matrices,” *Elsevier*, 2004.
- [34] Y. Kabashima, H. Takahashi, and O. Watanabe, “Cavity approach to the first eigenvalue problem in a family of symmetric random sparse matrices,” *Journal of Physics: Conference Series*, vol. 233, p. 012001, 2010.
- [35] I. Neri and F. L. Metz, “Eigenvalue outliers of non-hermitian random matrices with a local tree structure,” *Physical Review Letters*, vol. 117, no. 22, p. 224101, 2016.
- [36] V. A. R. Susca, P. Vivo, and R. Kühn, “Top Eigenpair Statistics for Weighted Sparse Graphs,” *Journal of Physics A: Mathematical and Theoretical*, vol. 52, no. 48, p. 485002, 2019.
- [37] I. Neri and F. L. Metz, “Spectral theory for the stability of dynamical systems on large oriented locally tree-like graphs,” *Physical Review Research*, vol. 2, no. 3, p. 033313, 2020.
- [38] O. Ajanki, T. Krüger, and L. Erdős, “Singularities of Solutions to Quadratic Vector Equations on the Complex Upper Half-Plane,” *Communications on Pure and Applied Mathematics*, vol. 70, no. 9, p. 1672:1705, 2017.
- [39] F. Benaych-Georges and R. R. Nadakuditi, “The eigenvalues and eigenvectors of finite, low rank perturbations of large random matrices,” *Advances in Mathematics*, vol. 227, no. 1, p. 494:521, 2011.
- [40] M. C. Munder, D. Midtvedt, T. Franzmann, E. Nüske, O. Oliver, M. Herbig, E. Ulbricht, P. Müller, A. Taubenberger, S. Maharana, L. Malinowska, D. Richter, J. Guck, V. Zaburdaev, and S. Alberti, “A pH-driven transition of the cytoplasm from a fluid- to a solid-like state promotes entry into dormancy,” *eLife*, vol. 5, p. e09347, mar 2016.
- [41] F. G. Quiroz, V. F. Fiore, J. Levorse, L. Polak, E. Wong, H. A. Pasolli, and E. Fuchs, “Liquid-liquid phase separation drives skin barrier formation.,” *Science*, vol. 367(6483), p. eaax9554, 2020.
- [42] R. Milo and R. Phillips, “Cell biology by the numbers,” *Garland Science*, 2015.
- [43] L. P. Kozłowski, “Proteome-pI: proteome isoelectric point database,” *Nucleic Acids Res.*, vol. 45(D1), no. 4, p. D1112:D1116, 2017.
- [44] B. Derjaguin and L. Landau, “Theory of the stability of strongly charged lyophobic sols and of the adhesion of strongly charged particles in solutions of electrolytes,” *Progress in Surface Science*, vol. 43, no. 1, p. 30:59, 1993.
- [45] J. Overbeek and E. J. Verwey, “Theory of the Stability of Lyphobic Colloids,” *Amsterdam: Elsevier*, 1949.
- [46] Wilson W. W. and L. J. Delucas, “Applications of the second virial coefficient: protein crystallization and solubility,” *Acta crystallographica. Section F, Structural biology communications*, vol. 70, p. 543:554, 2014.
- [47] J. Kiraga, P. Mackiewicz, D. Mackiewicz, M. Kowalczyk, P. Biecek, N. Polak, K. Smolarczyk, M. R. Dudek, and S. Cebrat, “The relationships between the isoelectric point and: length of proteins, taxonomy and ecology of organisms,” *BMC genomics*, vol. 8, 2007.
- [48] A. Quigley and D. R. Williams, “The second virial coefficient as a predictor of protein aggregation propensity: A self-interaction chromatography study,” *European Journal of Pharmaceutics and Biopharmaceutics*, vol. 96, p. 282:290, 2015.
- [49] J. R. Alford, B. S. Kendrick, J. F. Carpenter, and T. W. Randolph, “Measurement of the second osmotic virial coefficient for protein solutions exhibiting monomer-dimer equilibrium,” *Analytical biochemistry*, vol. 377, p. 128:133, 2008.
- [50] P. M. Tessier, S. I. Sandler, and A. M. Lenhoff, “Rapid measurement of protein osmotic second virial coefficients by self-interaction chromatography,” *Biophysical Journal*, vol. 82(3), p. 1620:1631, 2002.

- [51] O. Adame-Arana, C. A. Weber, V. Zaburdaev, J. Prost, and F. Jülicher, “Liquid Phase Separation Controlled by pH,” *Biophysical Journal*, vol. 119, no. 8, p. 1590:1605, 2020.
- [52] C. F. Lee, C. P. Brangwynne, J. Gharakhani, A. A. Hyman, and F. Jülicher, “Spatial organization of the cell cytoplasm by position-dependent phase separation,” *Physical Review Letters*, vol. 111, no. 8, p. 088101, 2013.
- [53] Z. D. Bai, “Methodologies in spectral analysis of large dimensional random matrices, a review,” in *Advances in statistics*, p. 174:240, World Scientific, 2008.
- [54] P. Bartlett, “Thermodynamic properties of polydisperse hard spheres,” *Molecular Physics*, vol. 97, no. 5, p. 685:693, 1999.
- [55] H. P. Erickson, “Size and Shape of Protein Molecules at the Nanometer Level Determined by Sedimentation, Gel Filtration, and Electron Microscopy,” *Biol Proced Online*, vol. 11, no. 32, 2009.